

## Supporting Information

### Simple Spray Deposition of the Water-based Superhydrophobic Coatings with High Stability for Flexible Applications

*Hui Ye<sup>a</sup>, Liqun Zhu<sup>a</sup>, Weiping Li<sup>a</sup>, Huicong Liu<sup>a</sup>, Haining Chen<sup>\*a</sup>*

- a. Key Laboratory of Aerospace Materials and Performance (Ministry of Education), School of Materials Science and Engineering, Beihang University, No. 37 Xueyuan Road, Haidian District, Beijing 100191, People's Republic of China.

\*Corresponding email: [chenhaining@buaa.edu.cn](mailto:chenhaining@buaa.edu.cn)

**Supplementary results:**

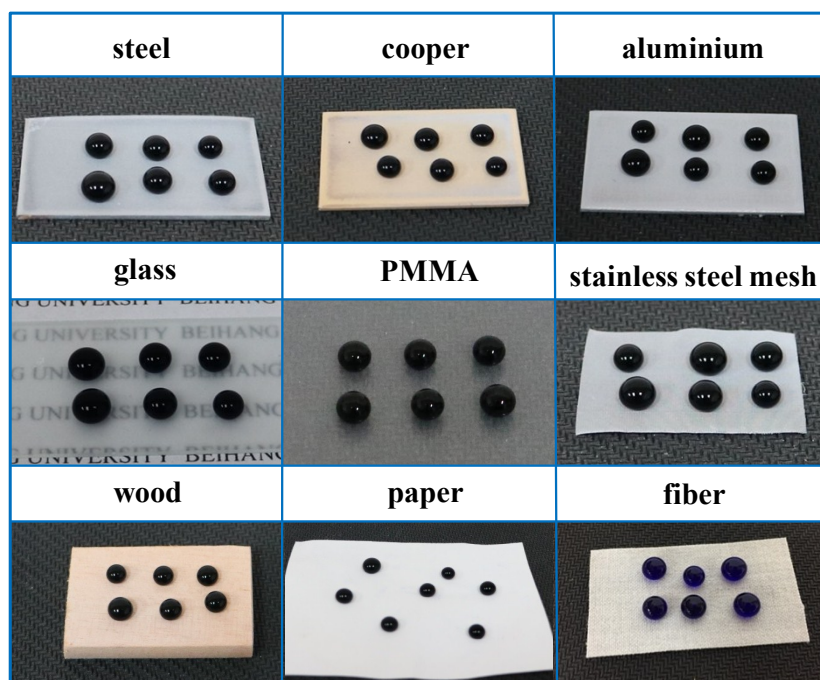
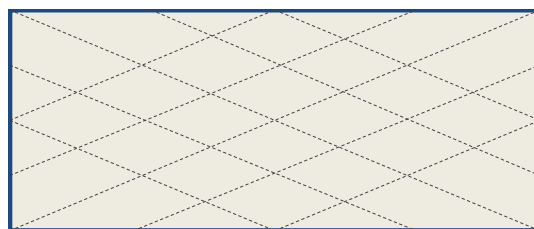


**Figure S1.** Water droplets placed on the composite superhydrophobic surfaces of various substrates.



- - - Knife scratch path

**Figure S2.** Schematic of knife-scratch setup

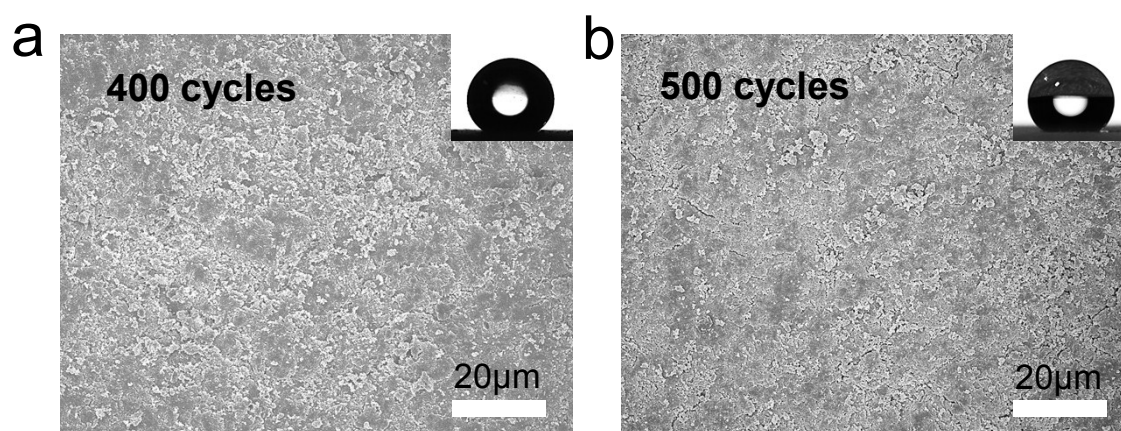


**Figure S3.** SEM images of the composite coatings after (a) 400 cycles of abrasion, (b) 500 cycles of abrasion. The inset is the water contact angle of the coating.

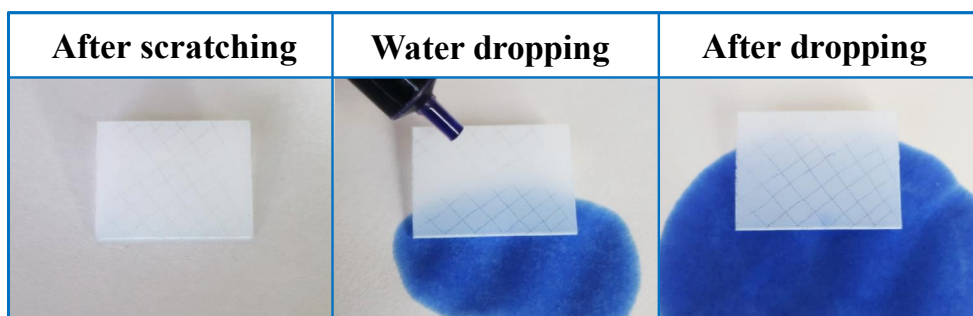


**Figure S4.** The composite superhydrophobic coating retained its water-repellent property even after knife scratches

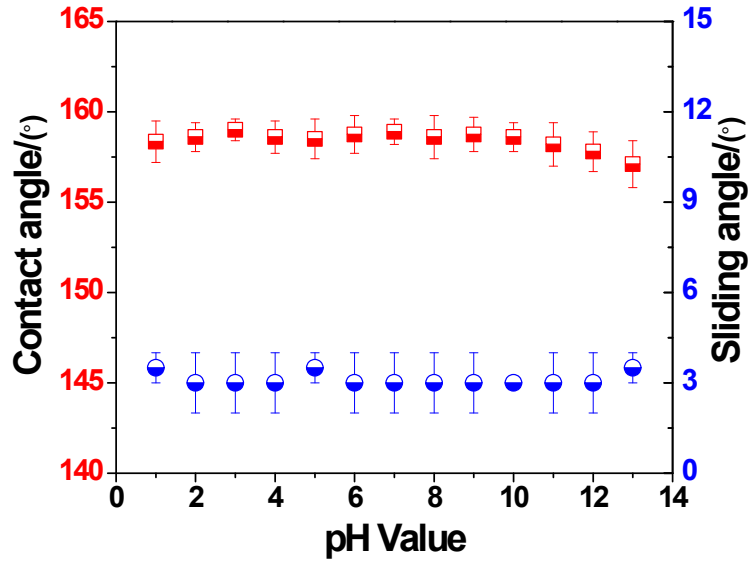


**Figure S5.** Water contact angles and sliding angles of the as-prepared superhydrophobic coating with different pH of aqueous solution immersion tests. The composite coatings still remain superhydrophobicity after immersion tests for 24h, demonstrated excellent pH-tolerant property.

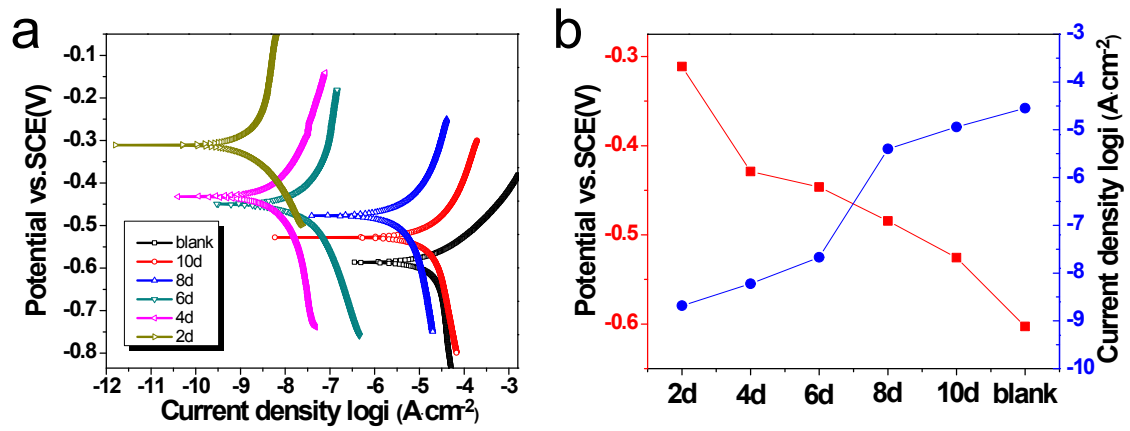


**Figure S6.** (a) Potentiodynamic polarisation curves of different immersion time in pH=1 hydrochloric acid aqueous solution. (b) Corrosion potentials and current densities panel of the samples with different immersion time

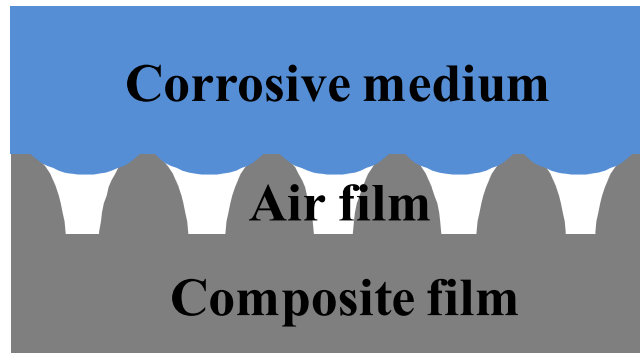


**Figure S7.** Interfacial model for chemical stability mechanism of the composite superhydrophobic coating in corrosive medium.

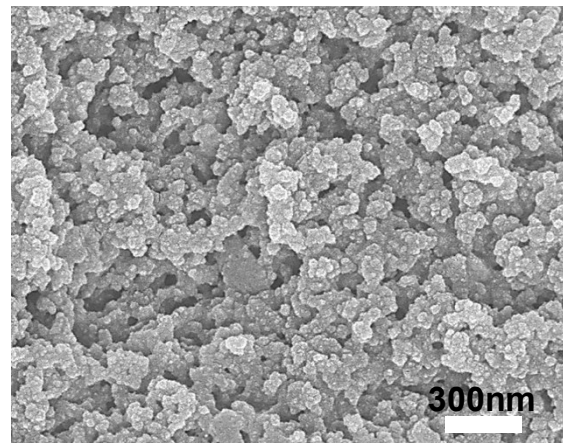


**Figure S8.** SEM image of the composite coating after immersion test for 6d.

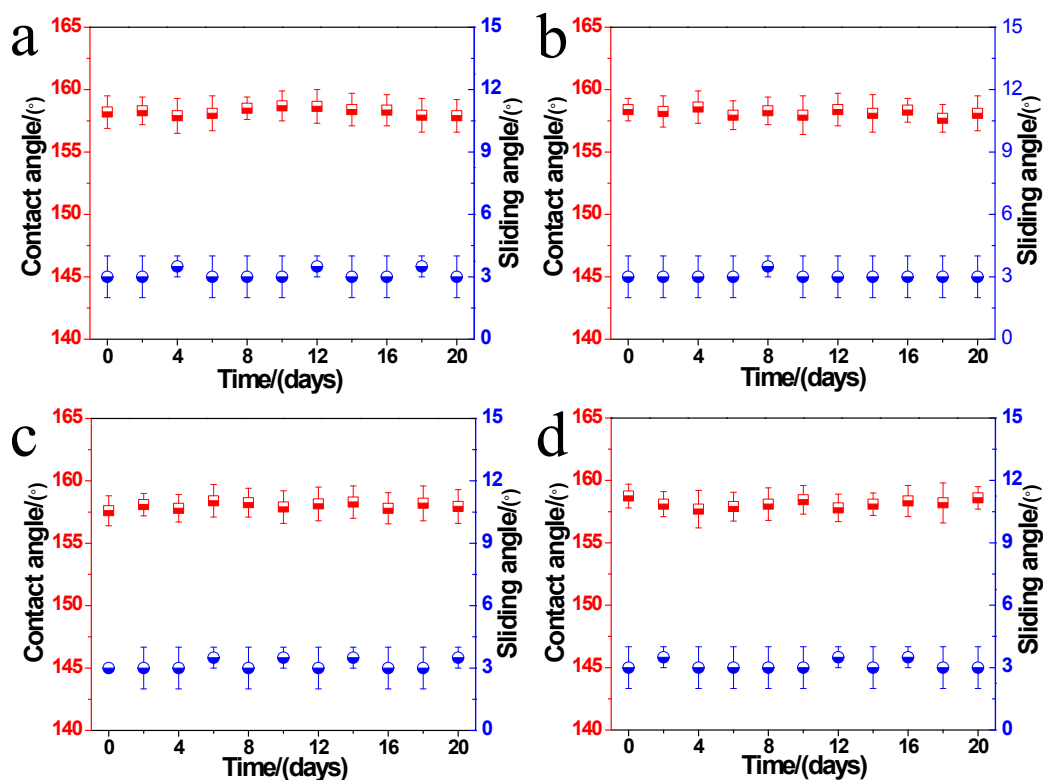


**Figure S9.** The water contact angles and sliding angles of the composite superhydrophobic coatings after solvent resistance tests for various time, a) acetone, b) butyl acetate, c) xylene, d) n-hexane.

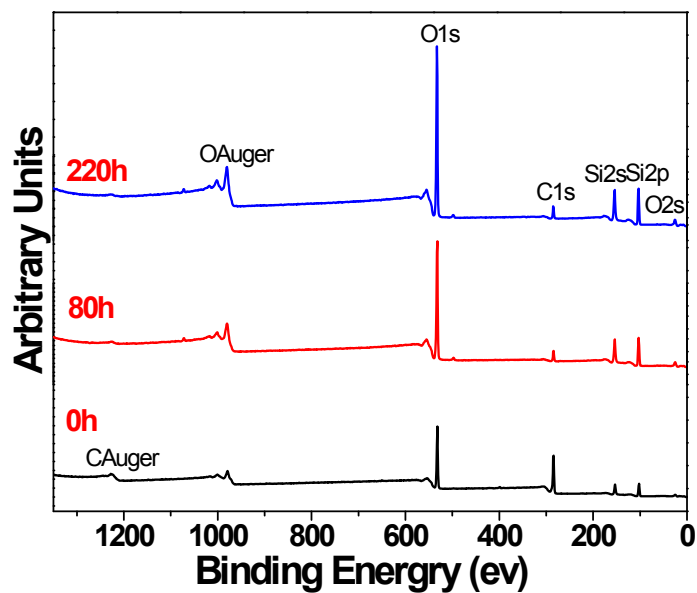


**Figure S10.** XPS spectra of the composite superhydrophobic coating before (0 hours) and after thermal stability test (annealed 80 and 220 hours at 400°C).

**Table S1.** Surface composition of the composite superhydrophobic coating before and after thermal stability test (annealed 80 and 220 hours at 400°C).

| Sample | Atomic percent (atom%) |       |       |
|--------|------------------------|-------|-------|
|        | C                      | O     | Si    |
| 0h     | 53.61                  | 31.05 | 15.33 |
| 80h    | 11.86                  | 56.65 | 31.49 |
| 220h   | 10.18                  | 58.31 | 31.51 |

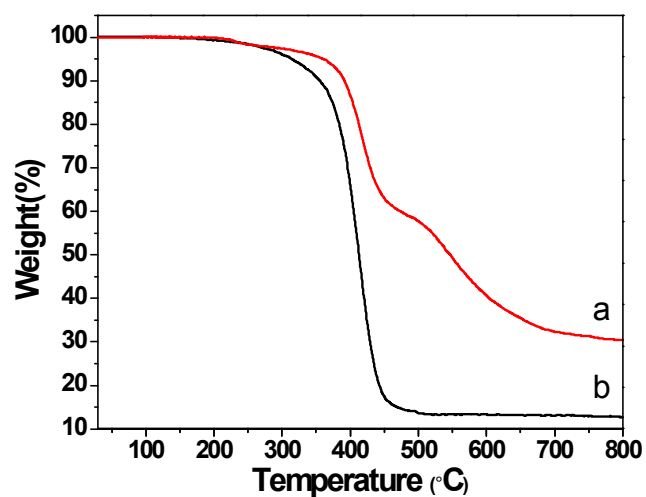


**Figure S11.** TGA curves of (a) the composite superhydrophobic coating, (b) the siloxane functionalized waterborne acrylic copolymer.



**Figure S12.** Image of a water droplet on the coated glass slide under oil, which still exhibits superhydrophobicity.

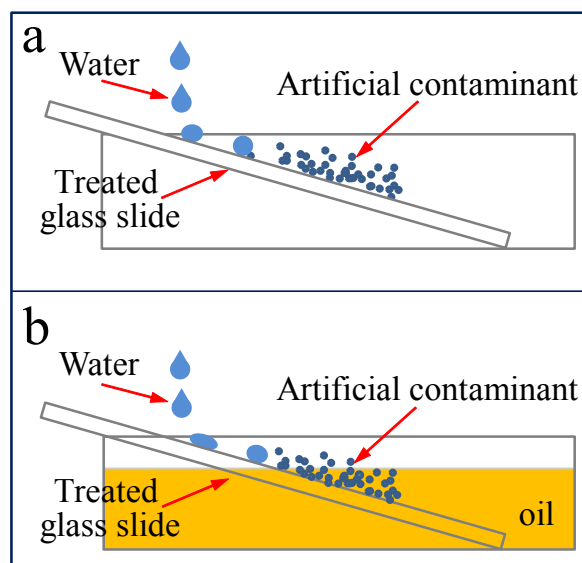


**Figure S13.** Schematic illustration of self-cleaning test. (a) Dirt removal test on coated surface in air. (b) Dirt removal test on oil-contaminated coated surface under oil.



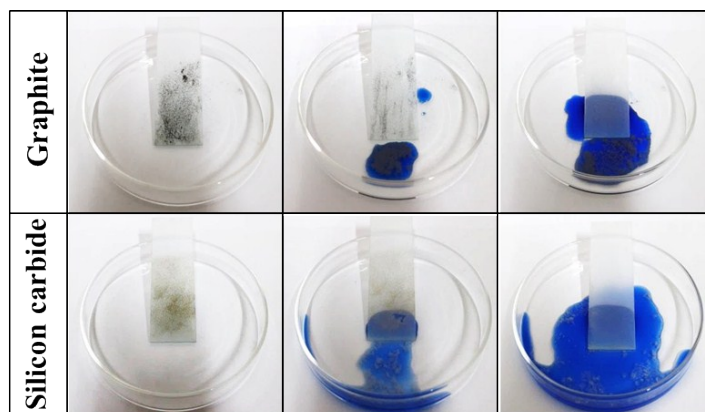
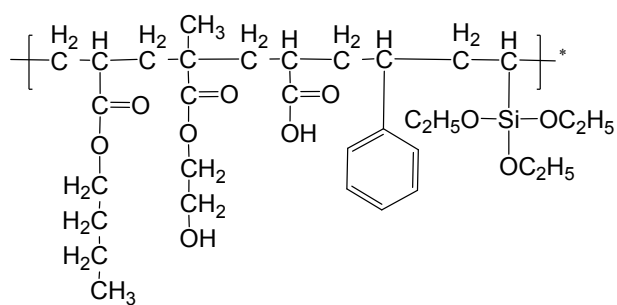


**Figure S14.** Self-cleaning action of the composite coatings performed on artificially contaminated surfaces with graphite and SiC particles in air.



**Scheme S1.** A schematic structure of typical silicone-acrylic copolymer

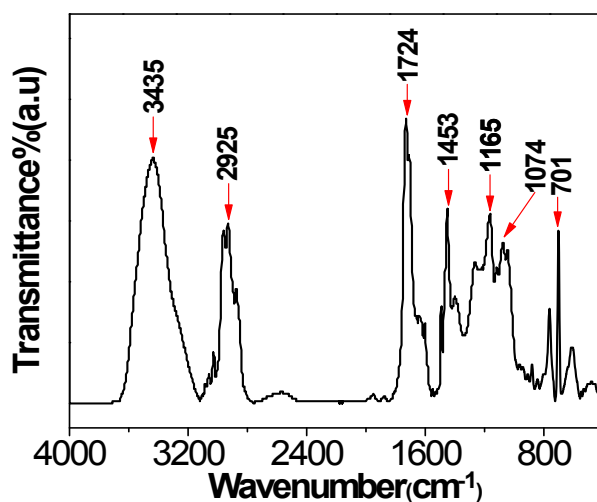


**Figure S15.** FT-IR spectrum of the silicone-acrylic copolymer (SAC)

Analysis on FT-IR result: The peak at  $3435\text{ cm}^{-1}$  is assigned to the stretching vibration of  $\text{-OH}$ , while the peaks from  $3100\text{ cm}^{-1}$  to  $3000\text{ cm}^{-1}$  correspond to the stretching vibration of  $\text{C-H}$  on the benzene ring. The peak at  $2925\text{ cm}^{-1}$  corresponds to the characteristic asymmetrical stretching vibration of  $\text{-CH}_2\text{-}$ , while the strong peak at  $1724\text{ cm}^{-1}$  is attributed to the stretching vibration of  $\text{C=O}$ . The peak at  $1453\text{ cm}^{-1}$  is due to the asymmetrical deformation vibration and symmetrical deformation vibration of  $\text{-CH}_3$ , whereas the peak at  $1165\text{ cm}^{-1}$  is assigned to the stretching vibration of  $\text{C-O-C}$  from esters. Besides, there exists an obvious peak at  $1074\text{ cm}^{-1}$ , which is well consistent with the characteristic stretching vibration peaks of  $\text{Si-O-C}$ .